Int. J. Heat Mass Transfer. Vol. 33, No. 7, pp. 1485–1496, 1990
Printed in Great Britain

0017–9310/90 $3.00 + 0.00

Numerical analysis of laminar mixed convection in horizontal internally finned tubes

I. M. RUSTUM and H. M. SOLIMAN
Department of Mechanical Engineering, University of Manitoba, Winnipeg, Manitoba, Canada R3T 2N2

(*Received* 6 *June* 1989 *and in final form* 28 *September* 1989)

Abstract—Steady, laminar, mixed convection in the fully developed region of horizontal internally finned tubes is investigated for the case of uniform heat input axially and uniform wall temperature circumferentially. The fluid flow and heat transfer characteristics are found to be dependent on a modified Grashof number Gr^+, Prandtl number Pr, number of fins M and the relative fin height H. Governing differential equations are solved numerically for the parametric range $M = 4$ and 16, $H = 0$, 0.2, 0.5 and 0.8, $Pr = 7$ and $Gr^+ = 0$ to 2×10^6. Computed results include the secondary flow components, axial velocity and temperature distributions, wall heat flux, friction factor and average Nusselt number. Internal finning is found to retard the onset of significant free convective effects and to suppress the enhancements in friction factor and Nusselt number compared to smooth tubes. Satisfactory agreement is obtained between the present numerical results and previous experimental data.

INTRODUCTION

THE NEED for compact heat exchangers has motivated extensive research into different methods of heat transfer augmentation. An attractive technique which has found wide use in industry is internally finned tubes. The enhancement achieved by these tubes over smooth tube conditions is particularly significant in laminar flow.

Many aspects of the pressure drop and heat transfer characteristics of internally finned tubes were considered in previous analytical (e.g. refs. [1–7]) and experimental (e.g. refs. [8–12]) investigations. These studies covered different tube geometries (fin height, number of fins, straight and spiral fins), both flow situations (laminar and turbulent) and the two extreme thermal boundary conditions (uniform heat input axially and uniform wall temperature axially). Most of the analytical studies were limited to the case of pure forced convection heat transfer. For turbulent flows, the forced convection models succeeded in predicting the experimental values of the friction factor and Nusselt number reasonably well [5]. However, experimental results in the laminar flow region (e.g. ref. [11]) have exhibited significant deviation from the forced convection models which may be attributed to the influence of free convection.

Due to the complexity of the flow cross-section, mixed convection in internally finned tubes was considered only in a limited number of analytical studies. Prakash and Patankar [13] solved numerically the case of fully-developed, laminar mixed convection in vertical tubes. This orientation simplified the analysis since the pertaining flow is purely axial and identical conditions exist in the bays formed by any two adjacent fins. Mirza and Soliman [14] analyzed mixed convection in the horizontal orientation; however, the cross-section was simplified by considering only two identical vertical fins. In both investigations, the presence of the fins was found to retard and suppress the free convective effects compared to smooth tubes.

The objective of this investigation is to extend the analysis for the horizontal orientation to a wide geometrical range in terms of fin heights and number of fins in order to produce results relevant to the tubes currently used in practice. The theoretical approach used here allows for the study of the detailed characteristics of fluid flow and heat transfer during laminar mixed convection. These details, which are difficult to study experimentally, are very useful in explaining the overall performance (friction factor and Nusselt number) of these tubes. The present predictions of the overall performance are compared with the available experimental data in order to assess the accuracy of this approach.

ANALYSIS

Formulation

The geometry under consideration is shown in Fig. 1. It consists of a horizontal, circular tube with a number of straight longitudinal fins evenly distributed around the inner circumference of the tube. Fins are assumed to be of negligible thickness with sides oriented radially within the tube cross-section. Therefore, the geometry is completely defined by two parameters: the number of fins M and the relative fin height H.

This analysis is applicable to steady, laminar flow of incompressible, Newtonian fluids. Constant fluid properties are assumed, except for the density which is temperature-dependent where buoyancy effects are considered. Axial conduction and viscous dissipation within the fluid are assumed to be negligible. The flow is assumed to be fully developed hydrodynamically and thermally with uniform heat input axially and uniform wall temperature (tube wall and fins) circum-

NOMENCLATURE

A	total surface area of fins and tube wall [m^2]
A_f	surface area of fins [m^2]
c_p	specific heat [$J\,kg^{-1}\,K^{-1}$]
D	tube diameter, $2r_0$ [m]
f	friction factor, defined by equation (10a)
$f\,Re_0$	product of the friction factor and Reynolds number at $Gr^+ = 0$
g	gravitational acceleration [$m\,s^{-2}$]
Gr^+	modified Grashof number, defined by equation (8d)
H	relative fin height, l/r_0
h	local heat transfer coefficient [$W\,m^{-2}\,K^{-1}$]
$\bar{h}$	averaged heat transfer coefficient [$W\,m^{-2}\,K^{-1}$]
k	thermal conductivity [$W\,m^{-1}\,K^{-1}$]
l	fin height [m]
M	number of fins
$\overline{Nu}$	average Nusselt number, defined by equation (9a)
$\overline{Nu}_0$	average Nusselt number at $Gr^+ = 0$
P'	dimensionless cross-sectional excess pressure, defined by equation (8c)
$\bar{P}$	dimensionless cross-sectional average pressure, defined by equation (8c)
p	pressure [$N\,m^{-2}$]
p'	cross-sectional excess pressure, defined by equation (1) [$N\,m^{-2}$]
$\bar{p}$	cross-sectional average pressure, defined by equation (1) [$N\,m^{-2}$]
Pr	Prandtl number
Q'	rate of heat input per unit length [$W\,m^{-1}$]
Q'_f	rate of heat transfer from the fins per unit length [$W\,m^{-1}$]
R	dimensionless radial coordinate, defined by equation (8a)
r	radial coordinate [m]
r_0	tube radius [m]
Ra^+	modified Rayleigh number, $Gr^+ \cdot Pr$
Re	Reynolds number, defined by equation (10c)
T	dimensionless temperature, defined by equation (8d)
T_b	dimensionless bulk temperature
t	temperature [K]
t_w	uniform wall temperature [K]
U	dimensionless axial velocity, defined by equation (8b)
U_m	dimensionless mean axial velocity
u	axial velocity [$m\,s^{-1}$]
u_m	mean axial velocity [$m\,s^{-1}$]
V	dimensionless radial velocity, defined by equation (8b)
V^*	transformed dimensionless radial velocity, defined by equation (8b)
v	radial velocity [$m\,s^{-1}$]
W	dimensionless angular velocity, defined by equation (8b)
w	angular velocity [$m\,s^{-1}$]
X	dimensionless axial coordinate, defined by equation (10c)
x	axial coordinate [m].

Greek symbols

β	coefficient of thermal expansion [K^{-1}]
θ	angular coordinate
μ	viscosity [$N\,s\,m^{-2}$]
ν	kinematic viscosity [$m^2\,s^{-1}$]
ρ	density [$kg\,m^{-3}$]
ρ_w	density at wall temperature [$kg\,m^{-3}$].

ferentially. Consequently, the three velocity components, the axial pressure gradient and the axial temperature gradient are all invariant in the flow direction. This analysis considers the case of heating, i.e. situations where the wall temperature is higher than the fluid temperature.

Governing equations

For this three-dimensional internal flow problem, we will follow a parabolized Navier–Stokes procedure [15] in which the pressure approximation quite widely used is given by

$$p(r,\theta,x) = \bar{p}(x) + p'(r,\theta) \tag{1}$$

where $\bar{p}$ is the cross-sectional average pressure, which is assumed to vary linearly in the x-direction while p', which is permitted to vary within the tube cross-section, provides the driving force for the secondary flow. The Boussinesq approximation was used in formulating the body-force terms in the momentum equations, i.e.

$$\rho = \rho_w[1 + \beta(t_w - t)]. \tag{2}$$

Using the approximations expressed by relations (1) and (2), the governing continuity, momentum and energy equations can be expressed in the following nondimensional form:

$$\frac{\partial V^*}{\partial R} + \frac{\partial W}{\partial \theta} = 0 \tag{3}$$

$$\frac{V^*}{R^2}\left[\frac{\partial V^*}{\partial R} - \frac{V^*}{R}\right] + \frac{W}{R^2}\left[\frac{\partial V^*}{\partial \theta} - RW\right] = -\frac{\partial P'}{\partial R} + \frac{2}{R}\left[\frac{\partial^2 V^*}{\partial R^2} - \frac{1}{R}\frac{\partial V^*}{\partial R} + \frac{1}{R^2}\frac{\partial^2 V^*}{\partial \theta^2} - \frac{2}{R}\frac{\partial W}{\partial \theta}\right] + 0.5Gr^+ T\cos\theta \tag{4}$$

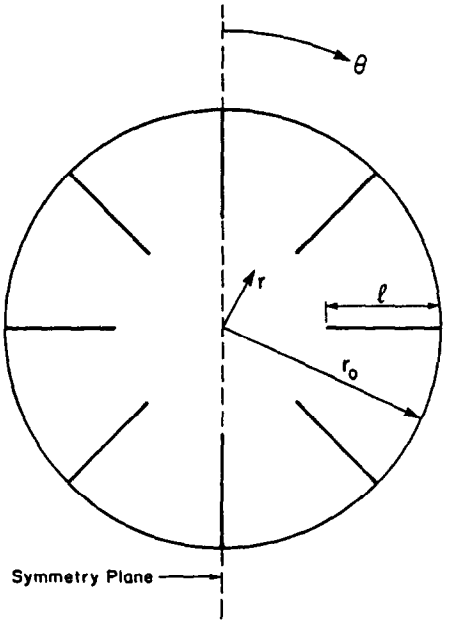

FIG. 1. Physical situation and coordinates.

$$\frac{V^*}{R}\frac{\partial W}{\partial R}+\frac{W}{R}\frac{\partial W}{\partial \theta}+\frac{V^*W}{R^2}=-\frac{1}{R}\frac{\partial P'}{\partial \theta}$$
$$+2\left[\frac{\partial^2 W}{\partial R^2}+\frac{1}{R}\frac{\partial W}{\partial R}-\frac{W}{R^2}+\frac{1}{R^2}\frac{\partial^2 W}{\partial \theta^2}+\frac{2}{R^3}\frac{\partial V^*}{\partial \theta}\right]$$
$$-0.5Gr^+ T\sin\theta \quad (5)$$

$$\frac{V^*}{R}\frac{\partial U}{\partial R}+\frac{W}{R}\frac{\partial U}{\partial \theta}=1$$
$$+2\left[\frac{\partial^2 U}{\partial R^2}+\frac{1}{R}\frac{\partial U}{\partial R}+\frac{1}{R^2}\frac{\partial^2 U}{\partial \theta^2}\right] \quad (6)$$

$$\frac{V^*}{R}\frac{\partial T}{\partial R}+\frac{W}{R}\frac{\partial T}{\partial \theta}=\frac{2}{Pr}\left[\frac{\partial^2 T}{\partial R^2}+\frac{1}{R}\frac{\partial T}{\partial R}+\frac{1}{R^2}\frac{\partial^2 T}{\partial \theta^2}\right]$$
$$-\frac{2}{Pr}\frac{U}{U_m} \quad (7)$$

where the dimensionless parameters used in equations (3)–(7) are given by

$$R=r/r_0, \quad Pr=\mu c_p/k \quad (8a)$$

$$U=\frac{u}{\frac{D^2}{2\mu}\left(-\frac{d\bar{p}}{dx}\right)}, \quad V^*=VR, \quad V=\frac{vD}{\nu}, \quad W=\frac{wD}{\nu} \quad (8b)$$

$$\bar{P}=\frac{\bar{p}}{\rho u_m^2}, \quad P'=\frac{p'D^2}{\rho\nu^2}+\frac{gD^2}{\nu^2}r\cos\theta \quad (8c)$$

$$T=\frac{t-t_w}{Q'/(\pi k)}, \quad Gr^+=\frac{g\beta Q'D^3}{\pi k\nu^2}. \quad (8d)$$

The above mathematical formulation indicates that the velocity, pressure and temperature distributions for a particular finned tube geometry (i.e. given M and H) are functions of the two independent parameters Gr^+ and Pr. Therefore, overall quantities, such as the friction factor and average Nusselt number, would also be dependent on M, H, Gr^+ and Pr. The average Nusselt number was calculated based on the definition

$$\overline{Nu}=\bar{h}D/k \quad (9a)$$

which reduces to the non-dimensional form

$$\overline{Nu}=-1/T_b \quad (9b)$$

while the friction factor was defined as

$$f=D(-d\bar{p}/dx)/(2\rho u_m^2) \quad (10a)$$

and in dimensionless form

$$f\,Re=-\frac{1}{2}\frac{d\bar{P}}{dX}=1/U_m \quad (10b)$$

where

$$X=x/(D\,Re), \quad Re=u_m D/\nu. \quad (10c)$$

The dimensionless mean velocity U_m and the dimensionless bulk temperature T_b were calculated from their respective standard definitions using Simpson's rule in evaluating the area integrals involved.

It must be pointed out that a transformed radial velocity V^* was used in equations (3)–(7) instead of the velocity V in order to invoke a strong boundary condition ($V^*=0$) at the centreline of the tube. Along the solid boundaries, the three velocity components and the temperature are equal to zero, while at the symmetry plane, the normal velocity component is equal to zero and the normal gradients of the other two velocity components and the temperature are equal to zero.

Solution technique

The present analysis assumes that, for any tube geometry, the uppermost fin is always oriented in a vertical direction. Therefore, a vertical plane passing through the tube centreline would always be a plane of symmetry for any tube geometry. Half of the tube cross-section would then constitute the solution domain.

Governing equations (3)–(7) were solved numerically using a control volume-based finite difference method [16]. A major feature of the present model is the strong coupling of pressure, velocity and temperature which was found to be troublesome particularly at high Grashof numbers. The SIMPLER procedure of Patankar [17] was used for handling the pressure–velocity coupling. Also, a line-by-line sweep was found necessary to avoid numerical divergence at moderate and high Gr^+. Starting from an initial guess,

Table 1. Values of $f\,Re$ and $\overline{Nu}$ for horizontal smooth tubes

	$Pr = 1$		$Pr = 7$	
Gr^+	$f\,Re$	$\overline{Nu}$	$f\,Re$	$\overline{Nu}$
0	15.98	4.367	15.98	4.367
10^4	16.59	4.705	16.15	6.007
10^5	19.97	6.388	16.90	9.076
10^6	26.35	9.350	18.67	13.93
2×10^6			19.52	16.04
10^∞	37.22	14.33		

Table 2. Values of $f\,Re_0$ and $\overline{Nu}_0$ for internally finned tubes

M	H	$f\,Re_0$	$\overline{Nu}_0$
4	0.2	18.54	4.570
	0.5	36.21	7.763
	0.8	71.30	19.60
16	0.2	26.55	4.747
	0.5	129.2	8.326
	0.8	440.7	110.2

the momentum and energy equations were solved simultaneously in order to determine a new value for all dependent variables at all mesh points along a radial line. After all radial lines have been swept successively in the angular direction, thus completing an iteration, the new set of velocities and temperature were compared with their corresponding values from the previous iteration. Convergence was assumed when the change in all velocity components and the temperature at all mesh points was within $\pm10^{-3}\%$, and the residual of the continuity equation at all mesh points was within $\pm10^{-3}$.

The solution domain was discretized using a mesh with even subdivisions in both the R- and θ-directions. The presence of the fins and their number had an influence on the number of subdivisions in the θ-direction required for good accuracy. After considerable experimentation using different meshes, the following mesh sizes were chosen (as a compromise between accuracy and computer time) in generating the final results:

smooth tube: 30×40 (radial × angular)

finned tubes ($M = 4$): 30×60

finned tubes ($M = 16$): 30×64.

Assessment of accuracy

Accuracy of the present results was assessed by comparing the predictions of the present numerical procedure (using the above mesh sizes) with previous results of some limiting cases. These limiting cases include forced and mixed convection in smooth tubes and forced convection in finned tubes. The comparisons involved values of $f\,Re$ and $\overline{Nu}$, as well as the velocity and temperature profiles for some cases.

For forced convection in smooth tubes the present model predicted $f\,Re_0 = 15.98$ and $\overline{Nu}_0 = 4.367$; both are within 0.13% of their respective exact values. Values of $f\,Re$ and $\overline{Nu}$ for mixed convection in horizontal smooth tubes are given in Table 1 for $Pr = 1$ and 7 over a range of Gr^+. Comparison was possible with the results of Hwang and Cheng [18] for $Pr = 1$ and Gr^+ up to 10^5 (which is the maximum value used in ref. [18]). The deviation in $f\,Re$ is always less than 0.3% and the deviation in $\overline{Nu}$ is generally within 1% but increases with Gr^+ up to a maximum of 2.4% at $Gr^+ = 10^5$. Comparisons were also made between sample results of the velocity and temperature distributions reported in ref. [18] and the present predictions. Excellent agreement was found in magnitude and trend.

The present values of $f\,Re_0$ and $\overline{Nu}_0$ for forced convection in internally finned tubes are shown in Table 2. Most of these results agree with those reported in refs. [1, 3] within 2% with a maximum deviation of 3%. It is to be noted that there is a deviation of up to 2.9% between the values of $f\,Re_0$ reported in refs. [1, 3] for the geometrical range (M and H) covered in Table 2.

In addition to the above comparisons, results of mixed convection in horizontal internally finned tubes were obtained for a few selected geometries using different mesh sizes for each geometry. When the values of $f\,Re$ and $\overline{Nu}$ were exponentially extrapolated to infinitesimal grid spacing it was found that the deviation between the results of the selected mesh and the extrapolated values was within 1.2% at all values of Gr^+. With such satisfactory results from all these tests and comparisons it was concluded that reasonable accuracy has been insured by the present numerical procedure.

RESULTS AND DISCUSSION

Solutions were obtained for finned tube geometries corresponding to $M = 4$ and 16, and $H = 0.2$, 0.5 and 0.8. A single value of Prandtl number, $Pr = 7$ (water), was used in all computations. For each tube geometry, results were obtained at different values of the modified Grashof number covering the range $0 \leqslant Gr^+ \leqslant 2\times10^6$. Computed results include the axial velocity and temperature distributions, the cross-sectional distributions of secondary velocity components and local wall heat flux, and the important overall quantities $f\,Re$ and $\overline{Nu}$. In the following presentation, detailed results for a representative sample of the cases studied are considered first, followed by a careful examination of the overall quantities and finally a comparison between the present numerical results and some previously published experimental data.

Secondary flow pattern

The pattern of the buoyancy-induced secondary flow is presented in the five parts of Fig. 2. These results correspond to $Pr = 7$ and $Gr^- = 2\times10^6$, i.e. $Ra^+ = 1.4\times10^7$. Figure 2(a), in which the smooth-

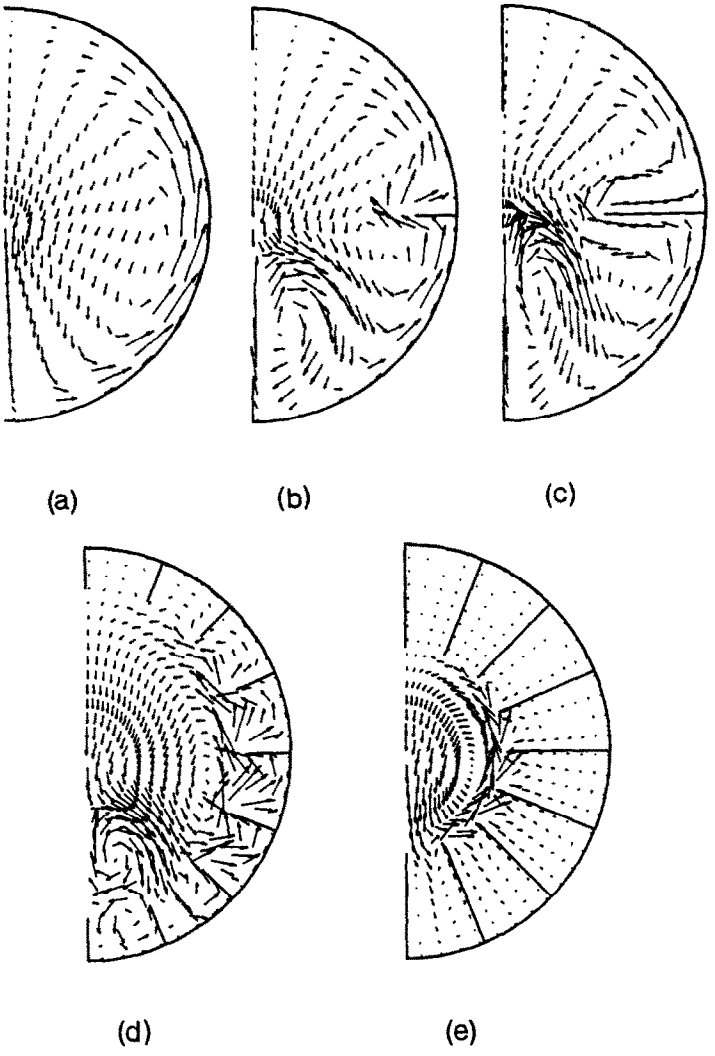

FIG. 2. Secondary flow pattern at $Gr^+ = 2 \times 10^6$, $Pr = 7$: (a) smooth tube; (b) $M = 4$, $H = 0.2$; (c) $M = 4$, $H = 0.5$; (d) $M = 16$, $H = 0.2$; (e) $M = 16$, $H = 0.5$.

tube case is considered, provides a reference for studying the influence of internal finning on the secondary flow pattern. These results show a single cell with upward flow along the heated wall and downward flow in the core. The absolute value of the secondary velocity vector along any radial line reaches a maximum near the wall.

The secondary flow pattern for a tube with a small number of short fins ($M = 4$ and $H = 0.2$) is shown in Fig. 2(b). Two counter-rotating secondary flow cells appear in the lower part of the tube, while in the upper part the flow pattern is close to the smooth-tube behaviour. An exchange of fluid exists between the top and bottom parts by upward moving flow around the tip of the horizontal fin and downward moving flow in the core. Higher secondary flow intensity can be seen in the lower part than the upper part of the tube. These trends continue as the fin height increases while keeping the same number of fins, as shown in Fig. 2(c).

For a large number of fins ($M = 16$), the secondary flow pattern is illustrated in Fig. 2(d) for short fins ($H = 0.2$) and in Fig. 2(e) for long fins ($H = 0.5$). Figure 2(d) shows a complicated pattern with two counter-rotating cells in the core of the tube and fluid exchange between core flow and each of the bays formed by two consecutive fins. In each bay, the exchange flow enters along the lower fin and exits along the upper fin. The intensity of secondary flow is always minimum in the uppermost bay and maximum in one of the lower bays, the exact location of which was found to depend on the modified Grashof number. For a large number of long fins, Fig. 2(e) shows a severely suppressed secondary flow in the bays formed by the fins. Many of the features shown in Fig. 2(e) are similar to those in Fig. 2(d) except for the reduced intensity and the disappearance of the second cell in the core. This second cell may form at higher Grashof numbers for this geometry.

The results presented in Fig. 2 demonstrate that

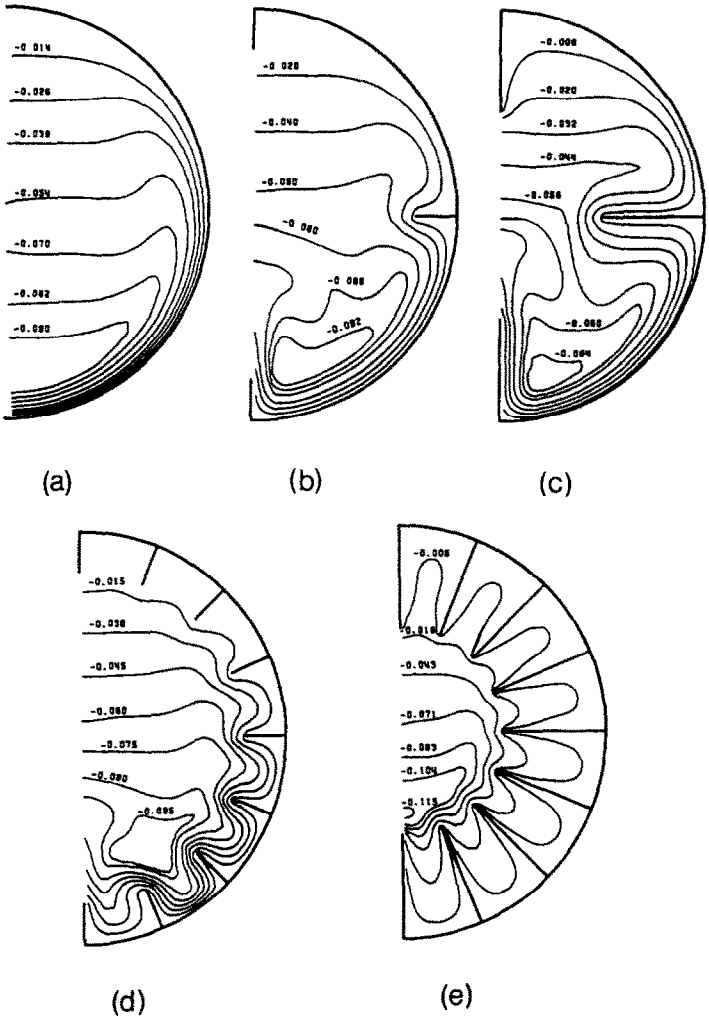

FIG. 3. Isotherms at $Gr^+ = 2 \times 10^6$, $Pr = 7$: (a) smooth tube; (b) $M = 4$, $H = 0.2$; (c) $M = 4$, $H = 0.5$; (d) $M = 16$, $H = 0.2$; (e) $M = 16$, $H = 0.5$.

internal finning has a strong influence on secondary flow in both magnitude and structure. These influences depend in a complicated way on the geometrical parameters H and M, and would naturally reflect on the remaining parts of the results.

Temperature distribution

The isotherms for some sample geometries are presented in Fig. 3 corresponding to $Gr^+ = 2 \times 10^6$ and $Pr = 7$. Figure 3(a) shows significant free convective effects for the smooth-tube case. The secondary flow circulation causes a large shift in the location of the minimum temperature from the tube centreline (during pure forced convection) downward along the symmetry plane. The local heat flux at the tube wall, which can be inferred from Fig. 3(a), was found to vary from a minimum at the top of the tube to a maximum at the bottom. Also, the absolute values of T are considerably lower than their forced convection values due to the cross-sectional circulation.

The case of a horizontal tube with a small number of short fins is exemplified in Fig. 3(b) for $M = 4$ and $H = 0.2$. During pure forced convection in this geometry, the temperature profile is identical in the upper and lower quarters separated by the plane of the horizontal fin, and the minimum temperature exists at the tube centre. The presence of natural circulation gives rise to a second minimum temperature in the lower quarter and it destroys the symmetry between the two quarters. It is also clear from Fig. 3(b) that the lower part of the tube wall becomes a much more effective heat transfer surface than the upper part. A general reduction in the fluid-to-wall temperature difference is experienced with free convection. Similar trends can be seen in Fig. 3(c) for $M = 4$ and $H = 0.5$.

At the same Grashof number, Figs. 3(d) and (e) show the free convective effects on the temperature distribution in tubes with a larger number of fins. With long fins, there is some degree of separation between the core area and the fin bays area. For example, with $M = 16$ and $H = 0.5$, Fig. 3(e) shows a core area with isotherms similar to those of a smooth tube and a number of bays with nearly similar temperature structure. The interaction between the core

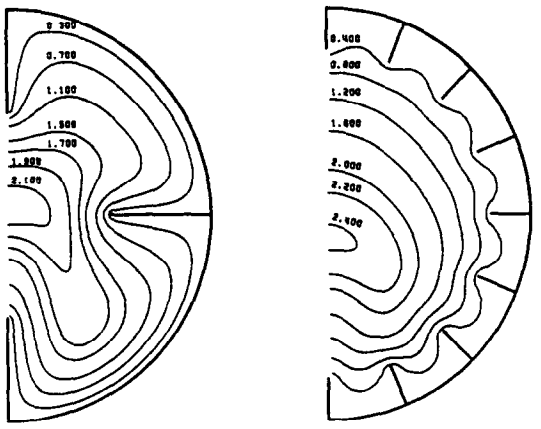

(a) (b)

FIG. 4. Isovels U/U_m at $Gr^+ = 2 \times 10^6$, $Pr = 7$: (a) $M = 4$, $H = 0.5$; (b) $M = 16$, $H = 0.2$.

and bays regions increases as the fin height decreases, as shown in Fig. 3(d). From this figure, it can also be noted that the amount of heat dissipation varies considerably among the fin bays with the second bay from the bottom providing the best performance.

Axial velocity distribution

For all geometries and all modified Grashof numbers, the influence of free convection on the axial velocity distribution was found to be less significant than the influence on temperature distribution. This trend is consistent with the smooth-tube results reported in previous investigations (e.g. ref. [18]) and would have an impact on the friction factor and Nusselt number, results which are presented later.

A sample of the present axial velocity distributions is presented in Figs. 4(a) and (b). The general trend in these results is for more mass concentration in the lower part of the tube than in the upper part. For very long fins ($H = 0.8$), the deviation in axial velocity from the forced convection case was found to be insignificant up to $Gr^+ = 2 \times 10^6$ (i.e. $Ra^+ = 1.4 \times 10^7$).

Distribution of wall heat flux

Figures 5 and 6 show the trend in the present results of local heat flux distribution at the solid wall (tube and fins). These results are presented in terms of $h/\bar{h}$, where h is the local heat transfer coefficient evaluated from the temperature gradient normal to the wall and $\bar{h}$ is the mean heat transfer coefficient over the whole solid surface.

Figure 5 corresponds to a finned tube with $M = 4$ and $H = 0.5$ and it shows the behaviour at $Gr^+ = 0$, 10^5 and 2×10^6. The abscissa is proportional to distance along the wall from the tip of the upper fin to the tip of the bottom fin in the direction shown in the inset of Fig. 5. At $Gr^+ = 0$, similarity exists between bays 1 and 2, as expected, and the areas near the tips of the fins are the most effective heat transfer surfaces. As Gr^+ increases, a higher proportion of the heat dissipation occurs in bay 2, which is consistent with the previous results of secondary flow and temperature distribution. A gradual decrease in relative heat transfer effectiveness can be seen at all the surfaces of bay 1 except for the area near the junction of the horizontal fin and the circular wall where some increase occurs. In bay 2, significant enhancement in heat transfer effectiveness is evident at the circular wall and the bases of the fins, while decreases in effectiveness occur near the fin tips. It must be pointed out that the results in Fig. 5 represent heat transfer at a particular wall location relative to the average heat transfer for each Gr^+. Therefore, caution must be exercised in interpreting these results since $\bar{h}$ depends on Gr^+, as shown later.

A second case is shown in Fig. 6 for $M = 16$, $H = 0.2$ and $Gr^+ = 0$, 10^5 and 2×10^6. The figure is simplified by including only the top bay and the bottom three bays since the behaviour at any point within the excluded bays was found to be consistent with a gradual monotonic change between the corresponding points in bays 1 and 2. As expected from the previous results, bay 3 (the second from the bottom) gets to be the most active at $Gr^+ = 2 \times 10^6$ while the top bay becomes the least active. The modified Grashof number can be seen to have a strong influence on the relative heat transfer effectiveness of different parts of the solid wall. Some similarities exist between Figs. 5 and 6 in terms of trend.

Another way of presenting the heat flux characteristics is shown in Fig. 7 in terms of Q_f'/Q', where Q_f' is the integrated sum of the heat transfer rate from the sides of the fins per unit axial length. For $M = 4$ and $H = 0.2$, Q_f'/Q' first decreases with Gr^+ and then increases gradually. An increase in either M or H causes an increase in the value of Gr^+ at which Q_f'/Q' starts decreasing. This is due to the fact that secondary flow is retarded within the bays by increases in either M or H, as shown earlier. Comparing Q_f'/Q' to A_f/A, which is the ratio of the total surface area of the fins to the total surface area of the solid wall, we find that the fins are more effective heat transfer surfaces for all the geometries in Fig. 7 at low Gr^+. With the decrease in Q_f'/Q' at high Gr^+, Q_f'/Q' becomes smaller than A_f/A for some geometries (e.g. $M = 4$, $H = 0.2$ and 0.5) which indicates that, on average, the circular wall becomes more effective than the fins. This trend may again reverse at Gr^+ higher than the values covered in this investigation, as suggested by the behaviour with $M = 4$ and $H = 0.2$ (where there is a gradual increase in Q_f'/Q' at high Gr^+).

Friction factor and Nusselt number

Values of $f\,Re/f\,Re_0$, where $f\,Re_0$ corresponds to pure forced convection for the same geometry, are presented in Fig. 8 with the smooth-tube case included for reference. These results show that $f\,Re/f\,Re_0$ remains equal to unity up to a critical Grashof number

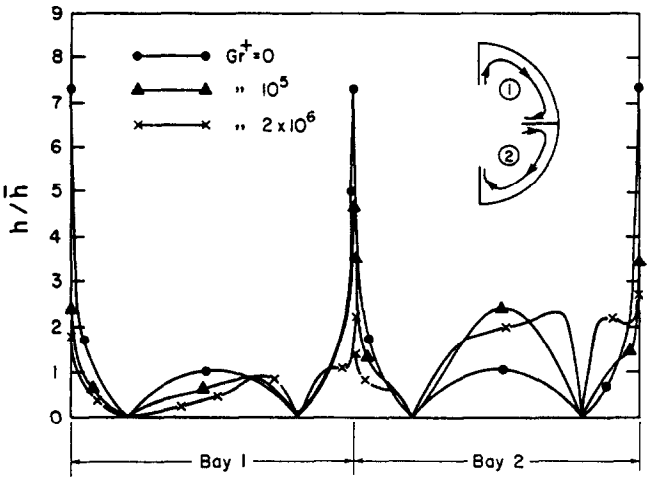

FIG. 5. Distribution of wall heat flux for $M = 4$, $H = 0.5$ and $Pr = 7$.

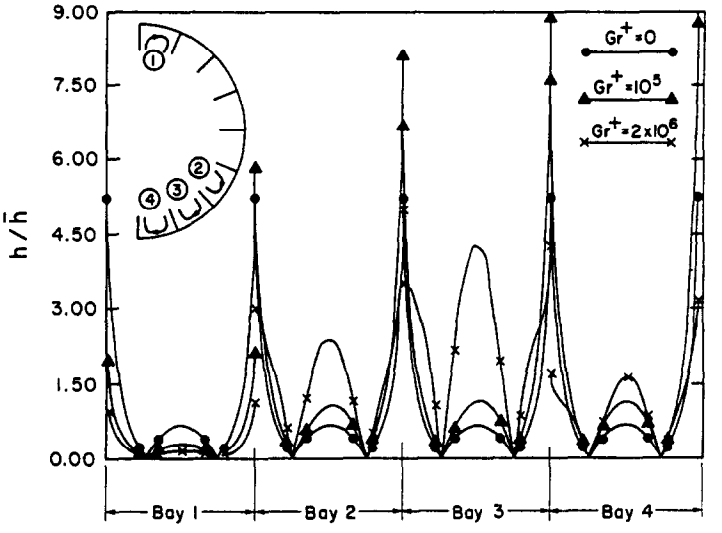

FIG. 6. Distribution of wall heat flux for $M = 16$, $H = 0.2$ and $Pr = 7$.

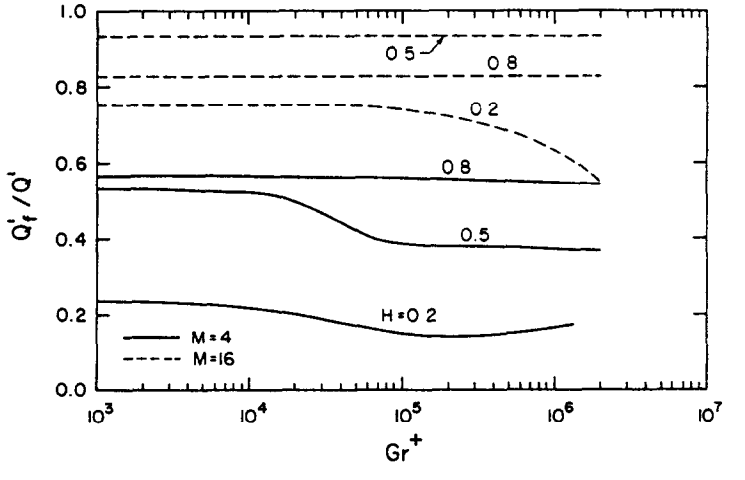

FIG. 7. Fractional fin heat dissipation as a function of Gr^+ ($Pr = 7$).

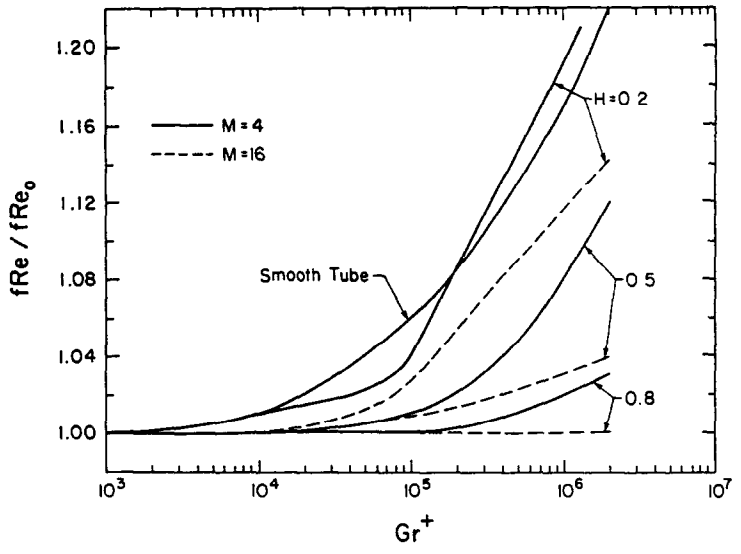

FIG. 8. The friction factor ratio as a function of Gr^+ ($Pr = 7$).

beyond which $f\,Re/f\,Re_0$ increases with Gr^+. This critical Gr^+ increases as either M or H increases, which can be attributed to the pattern by which the finning geometry retards the onset of secondary flow. Also, due to the fact that the presence of the fins generally suppresses the values of the secondary velocities, we find that the ratio $f\,Re/f\,Re_0$ decreases with increases in either M or H at any given Gr^+. For smooth tubes, the enhancement in the friction factor due to free convection exceeds that of finned tubes except for the geometry $M = 4$ and $H = 0.2$ at high Gr^+.

Figure 9 shows the variation of $\overline{Nu}/\overline{Nu_0}$ with Gr^+, where $\overline{Nu_0}$ is the pure forced convection value for the same geometry. The prevailing trends are similar to the ones discussed above in connection with the friction factor results. However, it must be noted that for any geometry, $\overline{Nu}/\overline{Nu_0}$ far exceeds $f\,Re/f\,Re_0$ at any Gr^+. This is consistent with the earlier results where it was shown that the influence of the free convective currents on the temperature distribution is much stronger than the influence on the axial velocity distribution. The manner by which variations in M and H influence $\overline{Nu}/\overline{Nu_0}$ is consistent with previously published experimental and theoretical results [11, 13, 14].

Comparison with experimental results

Predictions of the present theoretical investigation were compared with experimental data of fully-developed, laminar, mixed convection of water in horizontal internally finned tubes with uniform heat input axially [11]. This comparison is shown in Fig. 10 for a tube with $M = 16$ and $H = 0.318$, and in Fig. 11 for a tube with $M = 10$ and $H = 0.325$. In both

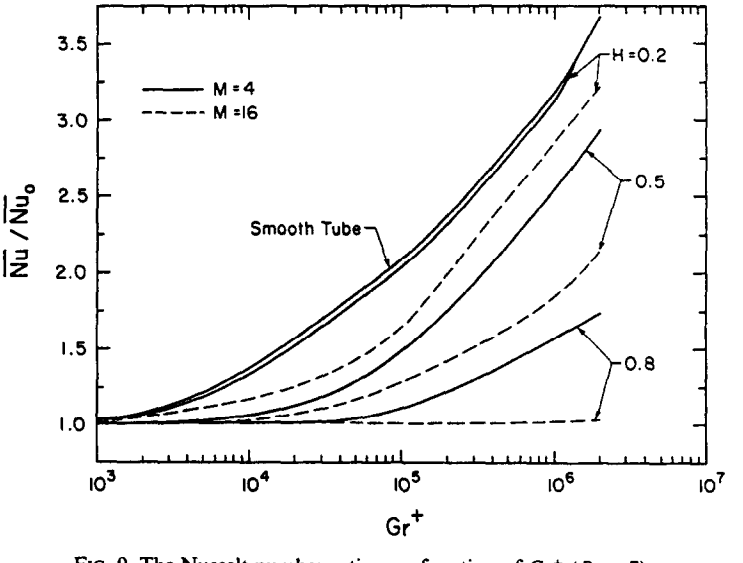

FIG. 9. The Nusselt number ratio as a function of Gr^+ ($Pr = 7$).

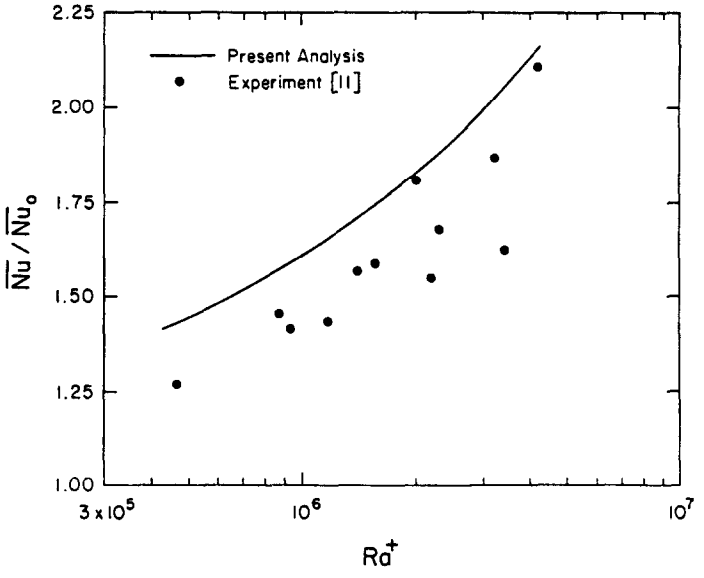

FIG. 10. Comparison of $\overline{Nu}/\overline{Nu}_0$ with experimental data for $M = 16$ and $H = 0.318$ ($Pr = 4.3$).

cases, the theoretical predictions were generated at a Prandtl number equal to the mean value for the respective data set. Only the values of $\overline{Nu}/\overline{Nu}_0$ were used in this comparison since $f\ Re/f\ Re_0$ were not reported in ref. [11].

Figures 10 and 11 show that the experimental data of $\overline{Nu}/\overline{Nu}_0$ are overpredicted by about 10–15%. It should be recalled that the present analysis assumes negligible fin thickness and uniform fin temperature (i.e. 100% fin efficiency). Both these assumptions result in slight overestimation of Nusselt number for the geometries considered in Figs. 10 and 11 [19]. Also, the experimental uncertainty in $\overline{Nu}$ was reported to be within $\pm 15\%$ [11]. Taking these factors into account, it may be concluded that the comparisons shown in Figs. 10 and 11 are quite satisfactory.

CONCLUDING REMARKS

A numerical analysis of laminar, fully-developed mixed convection in horizontal internally finned tubes has been presented encompassing a wide range of geometrical parameters. The results show that tube geometry (M and H) has a strong influence on the pattern and intensity of the secondary flow currents, which is in turn reflected on the axial velocity and temperature distributions, wall heat flux, friction factor and Nusselt number. In general, an increase in either M or H suppresses secondary flow in the bays formed by the fins at any given Grashof number. Consequently, the departure of $f\ Re$ and $\overline{Nu}$ from their respective forced convection values begins at higher Grashof numbers as M or H increases. This

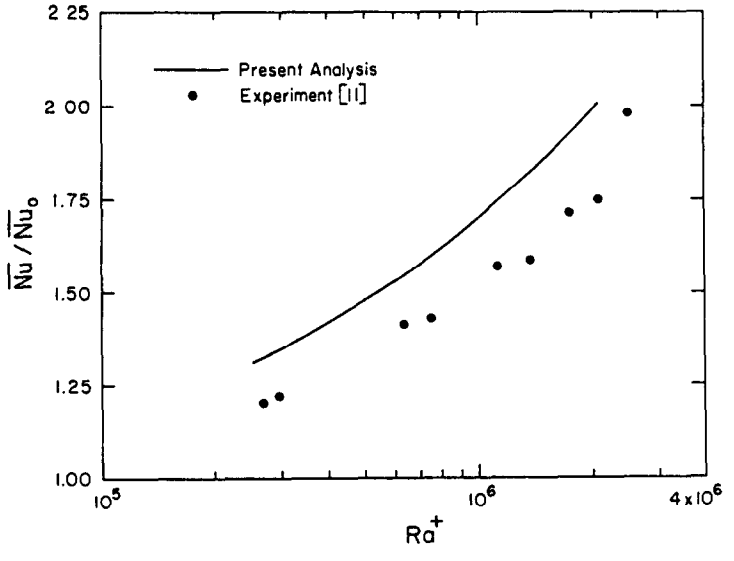

FIG. 11. Comparison of $\overline{Nu}/\overline{Nu}_0$ with experimental data for $M = 10$ and $H = 0.325$ ($Pr = 4.2$).

trend in the overall performance is consistent with previously reported experimental data [11] and is now justified by the detailed fluid flow and heat transfer characteristics presented in this investigation.

Acknowledgement—The financial assistance provided by the Natural Sciences and Engineering Research Council of Canada is gratefully acknowledged.

REFERENCES

1. M. H. Hu and Y. P. Chang, Optimization of finned tubes for heat transfer in laminar flow, *ASME J. Heat Transfer* **95**, 332–338 (1973).
2. J. H. Masliyah and K. Nandakumar, Heat transfer in internally finned tubes, *ASME J. Heat Transfer* **98**, 257–261 (1976).
3. H. M. Soliman and A. Feingold, Analysis of heat transfer in internally finned tubes under laminar flow conditions, *Proc. 6th Int. Heat Transfer Conf.*, Vol. 2, pp. 571–576 (1978).
4. H. M. Soliman, T. S. Chau and A. C. Trupp, Analysis of laminar heat transfer in internally finned tubes with uniform outside wall temperature, *ASME J. Heat Transfer* **102**, 598–604 (1980).
5. S. V. Pantankar, M. Ivanovic and E. M. Sparrow, Analysis of turbulent flow and heat transfer in internally finned tubes and annuli, *ASME J. Heat Transfer* **101**, 29–37 (1979).
6. C. Prakash and Y. D. Liu, Analysis of laminar flow and heat transfer in the entrance region of an internally finned circular duct, *ASME J. Heat Transfer* **107**, 84–91 (1985).
7. I. M. Rustum and H. M. Soliman, Numerical analysis of laminar forced convection in the entrance region of tubes with longitudinal internal fins, *ASME J. Heat Transfer* **110**, 310–313 (1988).
8. A. P. Watkinson, D. L. Miletti and G. R. Kubanek, Heat transfer and pressure drop of internally finned tubes in laminar oil flow, ASME Paper No. 75-HT-11 (1975).
9. W. J. Marner and A. E. Bergles, Augmentation of tube-side laminar flow heat transfer by means of twisted-tape inserts, static-mixer inserts, and internally finned tubes, *Proc. 6th Int. Heat Transfer Conf.*, Vol. 2, pp. 583–588 (1978).
10. T. C. Carnavos, Heat transfer performance of internally finned tubes in turbulent flow in advances in enhanced heat transfer, *ASME 18th Natn. Heat Transfer Conf.*, pp. 61–67 (1979).
11. I. M. Rustum and H. M. Soliman, Experimental investigation of laminar mixed convection in tubes with longitudinal internal fins, *ASME J. Heat Transfer* **110**, 366–372 (1988).
12. W. J. Marner and A. E. Bergles, Augmentation of highly viscous laminar heat transfer inside tubes with constant wall temperature, *Exp. Therm. Fluid Sci.* **2**, 252–267 (1989).
13. C. Prakash and S. V. Patankar, Combined free and forced convection in vertical tubes with radial internal fins, *ASME J. Heat Transfer* **103**, 566–572 (1981).
14. S. Mirza and H. M. Soliman, The influence of internal fins on mixed convection inside horizontal tubes, *Int. Commun. Heat Mass Transfer* **12**, 191–200 (1985).
15. D. A. Anderson, J. C. Tannehill and R. H. Pletcher, *Computational Fluid Mechanics and Heat Transfer*. McGraw-Hill, New York (1984).
16. S. V. Patankar and D. B. Spalding, A calculation procedure for heat, mass and momentum transfer in three-dimensional parabolic flows, *Int. J. Heat Mass Transfer* **15**, 417–440 (1972).
17. S. V. Patankar, *Numerical Heat Transfer and Fluid Flow*. McGraw-Hill, New York (1980).
18. G. J. Hwang and K. C. Cheng, Boundary vorticity method for convective heat transfer with secondary flow—application to the combined free and forced laminar convection in horizontal tubes, *Heat Transfer 1970*, Vol. 4, Paper No. NC 3.5 (1970).
19. H. M. Soliman, The effects of fin conductance on laminar heat transfer characteristics of internally finned tubes, *Can. J. Chem. Engng* **59**, 251–256 (1981).

ANALYSE NUMERIQUE DE LA CONVECTION LAMINAIRE MIXTE DANS DES TUBES HORIZONTAUX AILETES INTERIEUREMENT

Résumé—La convection permanente, laminaire, mixte dans la région pleinement établie d'un tube intérieurement aileté est étudiée dans le cas d'une entrée de chaleur axialement uniforme et d'une température pariétale uniforme sur la circonférence. Les caractéristiques de l'écoulement et du transfert de chaleur sont dépendantes du nombre de Grashof modifié Gr^+, du nombre de Prandtl Pr, du nombre d'ailettes M et de la hauteur relative d'ailette H. Les équations sont résolues numériquement pour le domaine paramétrique $M = 4$ et 16, $H = 0$, 0,2, 0,5 et 0,8, $Pr = 7$ et $Gr^+ = 0$ à 2×10^6. Les résultats du calcul incluent les composantes de l'écoulement secondaire, les distributions de la vitesse axiale et de la température, le flux thermique pariétal, le coefficient de frottement et le nombre de Nusselt moyen. L'ailetage interne retarde l'apparition des effets de convection libre et supprime l'amélioration du coefficient de frottement et du nombre de Nusselt, en comparaison du cas des tubes lisses. Un accord satisfaisant est obtenu entre les présents résultats numériques et les données expérimentales antérieures.

NUMERISCHE UNTERSUCHUNG DER LAMINAREN MISCHKONVEKTION IN WAAGERECHTEN, INNEN BERIPPTEN ROHREN

Zusammenfassung—Die stationäre laminare Mischkonvektion im Bereich vollständig entwickelter Strömung in einem horizontalen, innen berippten Rohr wird untersucht. Dabei wird der Fall gleichmäßiger axialer Wärmezufuhr und gleichmäßiger Wandtemperatur am Umfang betrachtet. Es zeigt sich, daß Strömung und Wärmeübergang von einer modifizierten Grashof-Zahl (Gr^*), der Prandtl-Zahl (Pr), der Anzahl der Rippen (M) und der relativen Rippenhöhe (H) abhängen. Die grundlegenden Differentialgleichungen werden numerisch im folgenden Parameterbereich gelöst: $M = 4$ und 16, $H = 0$; 0,2; 0,5 und 0,8; $Pr = 7$ und $Gr^* = 0$ bis 2×10^6. Folgende Größen werden berechnet: die Komponenten der Sekundärströmung, die Verteilungen von Geschwindigkeit und Temperatur, die Wärmestromdichte an der Wand, der Reibungsbeiwert und die mittlere Nusselt-Zahl. Es zeigt sich, daß die Innenberippung das Einsetzen einer spürbaren freien Konvektion verzögert; im Vergleich zu glatten Rohren wird die Erhöhung des Reibungsbeiwerts und der Nusselt-Zahl unterdruckt. Die Übereinstimmung mit früheren Versuchsergebnissen ist befriedigend.

ЧИСЛЕННЫЙ АНАЛИЗ ЛАМИНАРНОЙ СМЕШАННОЙ КОНВЕКЦИИ В ГОРИЗОНТАЛЬНЫХ ТРУБАХ С ВНУТРЕННИМ ОРЕБРЕНИЕМ

Аннотация—Исследуется установившаяся ламинарная смешанная конвекция в полностью развитой области горизонтальных труб с внутренним оребрением в случае аксиального подвода тепла и однородной по окружности температуры. Найдено, что характеристики течения жидкости и теплопереноса зависят от модифицированных чисел Грасгофа Gr^* и Прандтля Pr, количества ребер M и их относительной высоты H. Численно решаются определяющие дифференциальные уравнения для параметров $M = 4$ и 16, $H = 0$; 0,2; 0,5 и 0,8, $Pr = 7$ и $Gr^* = 0 - 2 \times 10^6$. Получены результаты для компонент скорости вторичного течения, аксиальной скорости и распределения температур, теплового потока на стенке, коэффициента трения и среднего значения числа Нуссельта. Найдено, что внутреннее оребрение затягивает порог заметного влияния свободной конвекции и подавляет рост коэффициента трения и числа Нуссельта по сравнению со случаем гладких труб. Получено удовлетворительное согласие между представленными численными результатми и известными экспериментальными, данными.